# An open-access computer image analysis (CIA) method to predict meat and fat content from an android smartphone-derived picture of the bovine 5th-6th rib

Bruno Meunier, Jérôme Normand, Benjamin Albouy-Kissi, Didier Micol, Mohammed El Jabri, Muriel Bonnet

Methods 186 (2021) 79–89

Contents lists available at ScienceDirect

Methods

journal homepage: www.elsevier.com/locate/ymeth

# An open-access computer image analysis (CIA) method to predict meat and fat content from an android smartphone-derived picture of the bovine 5th-6th rib

Bruno Meunier [a,*], Jérôme Normand [b], Benjamin Albouy-Kissi [c], Didier Micol [a], Mohammed El Jabri [d], Muriel Bonnet [a]

[a] Université Clermont Auvergne, INRAE, VetAgro Sup, UMR Herbivores, 63122 Saint-Genès-Champanelle, France
[b] French Livestock Institute, Carcass and Meat Quality Department, Agrapole, 23 rue Jean Baldassini, 69364 Lyon cedex 07, France
[c] Université Clermont Auvergne, CNRS, SIGMA Clermont, Institut Pascal, F-63000 Clermont-Ferrand, France
[d] French Livestock Institute, French Livestock Institute, Data Numeric Department, 149 rue de Bercy, 75595 Paris cedex 12, France

ARTICLE INFO

*Keywords:*
Marbling
Rib composition
Smartphone
Computer image analysis
Beef

ABSTRACT

Marbling and rib composition are important attributes related to carcass yields and values, beef quality, consumer satisfaction and purchasing decisions. An open-access computer image analysis method based on a fresh beef rib image captured under nonstandardized and uncontrolled conditions was developed to determine the intramuscular, intermuscular and total fat content. For this purpose, cross-section images of the 5th-6th rib from 130 bovine carcasses were captured with a Galaxy S8 smartphone. The pictures were analyzed with a program developed using ImageJ open source software. The 17 processed image features that were obtained were mined relative to gold standard measures, namely, intermuscular fat, total fat and muscles dissected from a rib and weighed, and intramuscular fat content (IMF - marbling) determined by the Soxhlet method. The best predictions with the lowest prediction errors were obtained by the sparse partial least squares method for both IMF percent and rib composition and from a combination of animal and image analysis features captured from the caudal face of the 6th rib captured on a table. These predictions were more accurate than those based on animal and image analysis features captured from the caudal face of the 5th rib on hanging carcasses. The external-validated prediction precision was 90% for IMF and ranged from 71 to 86% for the total fat, intermuscular and muscle rib weight ratios. Therefore, an easy, low-cost, user-friendly and rapid method based on a smartphone picture from the 6th rib of bovine carcasses provides an accurate method for fat content determination.

## 1. Introduction

Marbling can be defined as white flecks of intramuscular fat (IMF) distributed between muscle fibers. Marbling is one of the major attributes that determines the meat-eating qualities of beef and contributes to the economic value of carcasses and meat [1–3]. For example, the grading of carcasses in Asia and North America is influenced by the amount of marbling within certain limits; the more marbling there is, the higher the grade [4]. Thus, in the meat industry, a rapid, noninvasive and nondestructive evaluation and prediction of marbling is desired. The gold standard for marbling evaluation is the chemical analysis of intramuscular lipid content. However, the major drawbacks of this gold standard method are the destruction of a piece of muscle required for analyses as well as the time and cost of the analyses. Thus, alternative instrumental methods have been developed to manage and predict beef marbling, such as the application of tomography, ultrasound and visible–near-infrared spectroscopy to carcasses or muscles/meat as recently reviewed [5]; most of these methods are not cost-effective and require sophisticated instruments. Several imaging solutions have also been developed and applied to muscles to predict the marbling of beef breeds with high potential [6–10]. Imaging solutions have also been developed to predict the carcass yield from the morphometry of some muscles and major fat regions assayed from pictures of a rib cut [11–13]. Thus, imaging solutions have been suggested to provide accurate estimations of marbling and carcass composition, which are two major drivers of the economy for the beef industry. The prerequisite for these algorithm-

* Corresponding author.
*E-mail address:* bruno.meunier@inrae.fr (B. Meunier).

https://doi.org/10.1016/j.ymeth.2020.06.023
Received 15 April 2020; Received in revised form 18 June 2020; Accepted 30 June 2020
Available online 7 July 2020

based imaging solutions was, however, the quality of the pictures captured in controlled conditions in terms of the geometry, illumination and background to counteract the poor performances of the camera available and the difficulty of capturing images without artifacts. In recent years, smartphone image sensors have greatly progressed in terms of sensitivity, color precision and resolution and can now compete with professional cameras [14]. At the same time, the computation capacity of these devices has become similar to personal computers, which provides opportunities to develop computer vision apps. To date and to the best of our knowledge, imaging solutions have rarely been used from smartphone-based image processing to determine meat-eating quality attributes. Smartphone-based imaging solutions have been rarely developed for the evaluation of beef tenderness of fresh meat [15] or for the determination of fat content in deli products [16]. The main objective of this study is to report an open-access computer image analysis (CIA) method based on a fresh beef rib image captured with a smartphone under nonstandardized and uncontrolled conditions for estimating not only marbling but also rib composition in terms of muscle, total fat, intermuscular fat, intramuscular fat (i.e., marbling) and subcutaneous fat. The performances of the algorithms developed with open source tools were evaluated for measuring the multiscale fat distribution over the entire cross-section of a bovine rib photographed with a single smartphone in uncontrolled conditions such as on the carcass or after sampling. The obtained image analysis features were compared with gold standard methods, namely, IMF content and muscle and fat weight after rib dissection. Finally, data mining of all the features obtained provided prediction equations for the IMF in *longissimus thoracis* (LT) muscle, the total or intermuscular fat weight within the rib and the weight of LT muscle.

## 2. Material and methods

### 2.1. Animals

To produce the biological material required for good representativeness of the biological variability in marbling as well as the variability in the surface and shape of bovine ribs, 130 bovine ribs were collected from 7 dairy (mean slaughter age 20.4 months) and 31 beef (mean slaughter age 16.9 months) young bulls as well as 85 dairy (mean slaughter age 65.6 months) and 7 beef (mean slaughter age 73.0 months) cull cows, heifers or steers slaughtered in two slaughterhouses (Villers-Bocage, France, license number FR 14.752.10 CE and the experimental slaughterhouse of INRAE - UE1414 Herbipole, Theix, France). All animal trials described herein were conducted according to relevant international guidelines (European Union procedures on animal experimentation – Directive 2010/63/EU) for the use of production animals in animal experimentation. After slaughtering, carcasses were graded for conformation and fatness according to the EUROP grading system (Directive 1308/2013 UE), and hot carcass weight was recorded (Table 1). Carcasses were stored at 2–4 degreesC immediately after the slaughtering procedures, and carcasses were cut at the 5-6th rib at 24 or 48 h postmortem, which is the standard procedure for carcass management in France.

**Table 1**
Carcass characteristics (mean ± standard deviation) of the 130 bovines used in the study.

| | Dairy young bulls | Beef young bulls | Dairy others[1] | Beef others[1] |
|---|---|---|---|---|
| Number of bovine | 7 | 31 | 85 | 7 |
| Slaughter age (month) | 20.4 ± 1.9 | 16.9 ± 3.7 | 65.6 ± 25.1 | 73.0 ± 39.9 |
| Hot carcass weight (kg) | 369 ± 37 | 336 ± 83 | 352 ± 57 | 372 ± 42 |
| Conformation score[2] | P+ | R= | P+ | R− |
| Fat score[2] | 3.0 ± 0.0 | 2.9 ± 0.3 | 2.9 ± 0.4 | 3.0 ± 0.0 |

[1] Others: cull cows, heifers, steers.
[2] Conformation and fat scores according to the EUROP scale: from P- (poor) to E+ (excellent) for the carcass conformation and from 1 (very low) to 5 (very high) for the degree of carcass fatness.

### 2.2. Image acquisition

Cross-section images of the 6th rib were captured with a Galaxy S8 smartphone (® Samsung Electronics Co., South Korea) using the default settings except for the strobe, which was always active (Fig. 1-A). To reduce the specular reflexion [10], the smartphone was equipped with a protective cover on which two linear polarizers (® Edmund optics, United States of America) were fixed orthogonally, the first in front of its camera and the second in front of its strobe. A homemade laminated scale of 5 × 5 $cm^2$ (Fig. 1-B) was designed for calibrating the image geometrically. Each operator had to place the scale flat on the rib bone extremity, and he was instructed to photograph the rib perpendicularly to the cross-section. This operation was facilitated by the large display of the smartphone. Two pictures of each animal were captured. The cranial face of the 6th rib cross-section corresponding to the caudal face of the 5th rib (CAF5R) was captured directly on the front carcass, as it is traditionally hung in the slaughtering house (Fig. 1-C). The caudal face of the 6th rib (CAF6R) cross-section was captured on a red or white table available in the slaughterhouse (Fig. 1-D) once the rib was separated from the hindquarter (prepared rib, according to the United Nations Economic Commission for Europe (UNECE) code 1604). Each RGB (red, green, blue) image of 4032 × 3024 pixels was saved in the default JPEG format. With such recommendations, the spatial resolution would reach 100 μm, which is adapted for sampling even the small marbling flecks [6], and the perspective effect would be reduced.

### 2.3. Image analysis

A dedicated program was developed in macro language using open source ImageJ v1.52i image processing software [17] enriched with two packages (Auto_Threshold.jar, Fast_Morphology.jar). An operator was trained, and the operations concerning fat detection were automated to make the analysis more rapid and reproducible. The resulting images from each step of the following algorithm are illustrated in Fig. 1. The specific ImageJ functions are in italics.

#### 2.3.1. Image preprocessing

After loading and zooming on the scale of the raw RGB image (Fig. 1-C), the operator precisely spots the four corners of the 5 × 5 $cm^2$ scale. Then, perspective correction is carried out (*Landmark Correspondences*) followed by the geometrical calibration (*Set Scale*) of the image (Fig. 1-E). The most contrasted green (G) and blue (B) components are averaged to produce a grayscale image (Fig. 1-F). The commonly used median filter is then applied to eliminate the remaining noise.

#### 2.3.2. Semiautomatic segmentation of the anatomic areas of interest

Regardless of the slaughterhouse, the visible cross-section area from the prepared rib (UNECE code 1604) is often incomplete and relatively variable in size due to the way the hindquarters are cut. With the aim of realizing standardized area measurements, we propose to cut the rib again at seventy degrees (Fig. 1-E). This approach was preferred to a cut using anatomic landmarks [12] that were difficult to identify in a significant number of our images. Using a polygon pen, the operator roughly draws a large area around the intermuscular fat and the subcutaneous fat area adjoining the M. *trapezius thoracis* (Fig. 1-E). Then, he precisely draws (1) the rib portion, including M. *spinalis*, M. *multifidus*, M. *longissimus*, M. *iliocostalis*, M. *semispinalis capitis*, and M. *rhomboideus* and (2) the rib eye (or M. *longissimus*) (Fig. 1-F). Both areas are labeled to be analyzed geometrically (Fig. 1-G). The rib eye area is automatically (1) reduced (*Erode*) to 1.5 mm thickness (using successive erosion) to

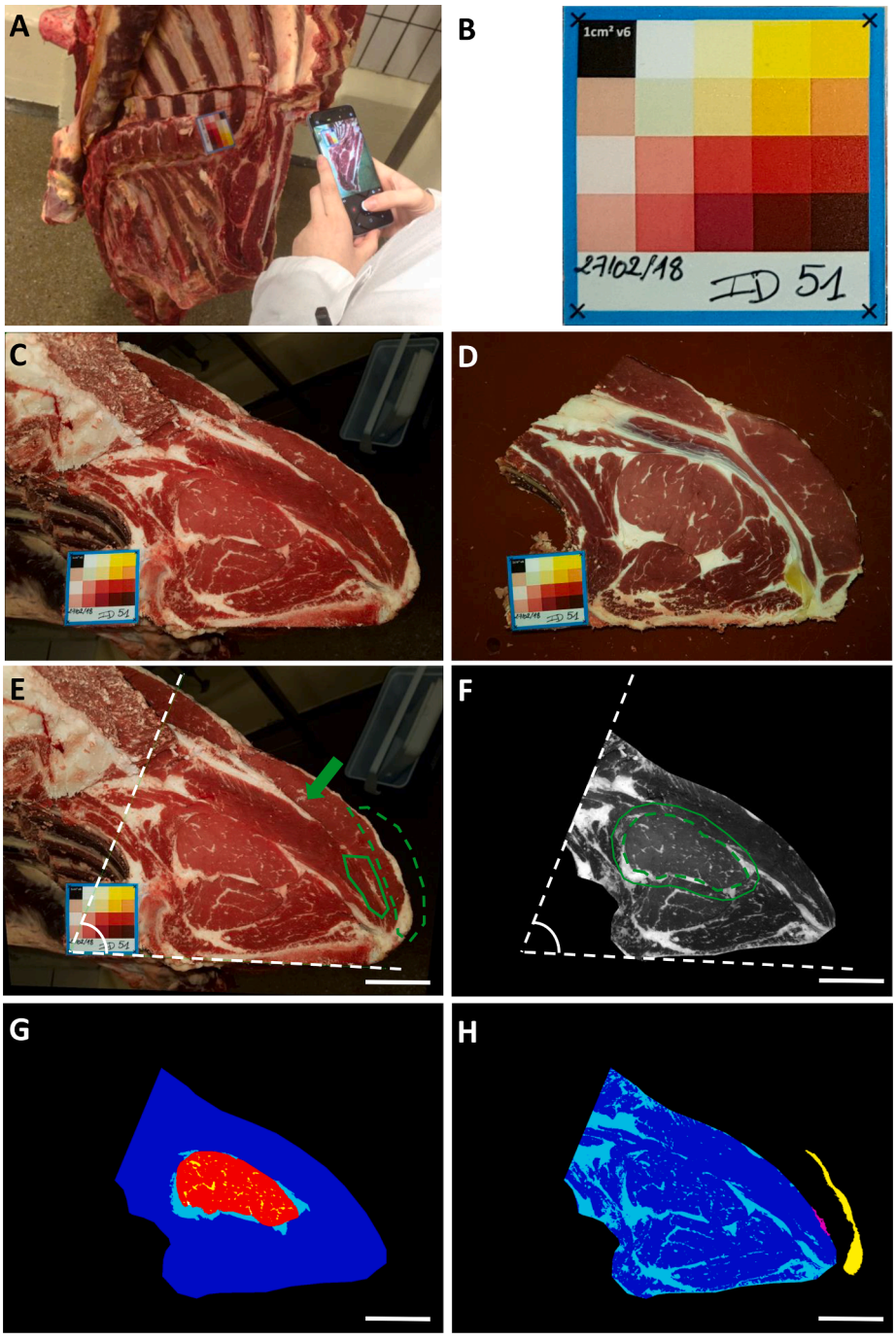


**Fig. 1.** Image acquisition (A-D) and processing (E-H). (A) General view of the shooting conditions on one hanging carcass. (B) Laminated scale of 5 × 5 $cm^2$ prepared for the carcass identified as ID51. (C) Caudal face of the 5th rib (CAF5R) captured on the hanging ID51 carcass. (D) Caudal face of the cut 6th rib (CAF6R) captured on the table. (E) ID51-CAF5R image corrected for perspective effects, geometrically calibrated (Scale bare = 5 cm) and cut at 70 degrees. The intermuscular fat (green polygon) and the subcutaneous fat (dashed green polygon) area adjoining the M. *trapezius thoracis* (green arrow) and starting from the bone were roughly drawn by the operator. (F) Rib portion area cut at 70 degrees (dashed white lines) excluding the bone and the M. *trapezius thoracis* and converted to grayscale. The rib eye was precisely drawn (green dashed polygon). Rib eye area automatically enlarged by 25% (green polygon). (G-H) Labeled image of automatically detected fat regions. (G) Intramuscular fat (yellow) in the rib eye (red) and intermuscular fat (cyan) in the rib eye area enlarged by 25%. (H) Total fat (cyan) in the rib portion (blue). Intermuscular fat area (pink) and the piece of subcutaneous fat area (yellow) adjoining the M. tra*pezius thoracis*. (For interpretation of the references to color in this figure legend, the reader is referred to the web version of this article.)

avoid the presence of intermuscular fat in the dissected rib eye area and (2) enlarged (*Enlarge*) by 25% (in proportion to the rib eye radius, corresponding to 65% in proportion to the rib eye area) to capture a proportional area of intermuscular fat all around the rib eye.

*2.3.3. Automatic segmentation of fat and lean region in the anatomic areas of interest*

With the aim of detecting areas related to the intramuscular (marbling), intermuscular and subcutaneous fat, which correspond to the brightest pixels in the grayscale image (Fig. 1-F), we evaluated several local or global thresholding methods available under ImageJ in a previous study. First, we retained those segmentation methods based on the image histogram analysis inside the rib eye enlarged by 25%. This area appeared optimal to maximize the chance of obtaining a significant proportion of the brightest pixels, even in lean animals. Then, we compared (1) the Otsu [18] and the MaxEntropy [19] methods, which have already been suggested to perform well for the automatic detection of marbling flecks [9], and (2) the Li [20] method, which, in our conditions, appeared to be intermediate in terms of over- or under-segmentation of the fat areas. According to visual inspection, the Li method (*Auto Threshold*) was proven to be more powerful, and its grayscale threshold was applied to detect (1) the intramuscular fat in the rib eye and intermuscular fat in the rib eye enlarged by 25% (Fig. 1-G), (2) the total fat in the rib portion and (3) the intermuscular fat and the subcutaneous fat area adjoining the M. *trapezius thoracis* in both drawn areas (Fig. 1-H). Manual thresholding by the operator was also achieved for the intramuscular fat in the rib eye [21].

#### 2.3.4. Image analysis and feature extraction

The entire segmented image was labeled (Fig. 1-G plus Fig. 1-H). The geometrical measurements (area, Feret diameter, perimeter and number of particles) were processed (*Analyze Particles*), and features were calculated mainly as area proportions [7] and were reported (Table 2). The boundaries of all segmented areas were placed in the overlay of the original image corrected for perspective effects, which was saved for further visual validation by an external expert.

### 2.4. Gold standard assays

The sixth ribs were cut using the thoracic vertebras as reference. The resulting rib thicknesses varied from approximately 4 to 6 cm depending on the bovine morphology and was not precisely recorded in this study. After the ribs were prepared (UNECE code 1604) and photographed, they were weighed (RibW) and dissected. Intermuscular fat, total fat, muscles and bones were separated from each other and weighed. Therefore, the fat to rib weight ratio (RibFatWR), muscle to rib weight ratio (RibMuscWR), intermuscular fat to rib weight ratio (RibInterWR) and intermuscular fat to LT weight ratio (RibInterWM) were calculated (Table 2). The weight of the LT muscle (LTW), also called the rib eye, was also recorded. The LT of the 6th rib was ground to obtain homogenous samples used for chemical analysis of marbling. The IMF content was assayed according to the Soxhlet method after acid hydrolysis. A well-defined and weighted amount (approximately 5 ± 0.001 g) of ground meat was hydrolyzed with 4 N hydrochloric acid for 1 h at 100 degreesC and then washed with water. Lipid extraction was achieved using an accelerated solvent extractor with 150 mL petroleum ether. After evaporation of the solvent, the flasks with the fat were dried for 3 h at 103 degreesC, cooled to room temperature in a desiccator and then weighed (±0.001 g) to determine the amount of IMF in the meat sample. The results were expressed as the % of IMF in fresh meat.

### 2.5. Data analysis

Statistical analysis was performed using R 3.5.1 software (https://r-project.org). Pearson correlation matrices between all 26 numerical parameters assayed on 130 bovines were processed and visualized. Prediction models were developed to predict the 7 gold standard parameters using two animal or carcass traits (age and HCW) and seventeen image analysis features for a total of 19 quantitative variables. To consider the qualitative animal variables, breed types («dairy» and «beef cattle» modalities) and maturity («young bull» and «others» modalities) were combined in a single variable according to four modalities («dairy young», «dairy others», «beef young», «beef others»). Due to the divergences among the number of bovines within the four modalities, virtual bovine's samples were then generated based on Synthetic Minority Oversampling Technique (SMOTE algorithm). SMOTE algorithm allowed oversampling the minority classes and redressing the class imbalance problem. This allowed reaching about 84 bovines by modality. The method was also very useful for splitting data into training (75% of the entire dataset) and validation sets (25% of the entire dataset) with an equilibrium among the four modalities. A total of 252 (84 bovines × 4 modalities × 75%) samples were used for training the prediction model. The remaining 84 samples were used for external validation.

Three machine learning approaches were compared to develop predictive models: sparse partial least squares (SPLS), random forest (RF) and the combination of clustering of variables and multiple linear regression (ClustOfVar + MLR). Unlike partial least squares regression, which reduces the dimensions and employs all predictors regardless of their relevance, the SPLS method allows both variable selection and dimension reduction. This method was thus chosen for its good predictive performance and was launched using the *mixOmics* R package [22]. Furthermore, the RF technique was also employed for the same purpose. A random forest consists of a large number of individual

**Table 2**
Animal characteristics and overview of all measurements (mean ± standard deviation) carried out on the 130 bovines used in this study and their images, (1) the cranial face of the 6th rib cross-section corresponding to the caudal face of the 5th rib (CAF5R - on carcass) and (2) the caudal face of the 6th rib (CAF6R - on table).

| Features | Description | Unit | Statistics | |
|---|---|---|---|---|
| | **Animal and carcass traits** | | | |
| Type | Breed type (dairy / beef cattle) | | | |
| Mat | Maturity (young bull / others) | | | |
| Age | Slaughter age | months | 51.9 ± 31.4 | |
| HCW | Hot carcass weight | kg | 350.2 ± 62.7 | |
| | **Gold standard parameters** | | | |
| IMF | Intramuscular fat in M. longissimus thoracis (rib eye) | % | 6.6 ± 3.6 | |
| RibFatWR | Rib Fat Weight Ratio (Rib fat weight divided by the rib weight) | % | 12.3 ± 4.8 | |
| RibMuscWR | Rib Muscle Weight Ratio (Rib muscle weight divided by the rib weight) | % | 66.1 ± 4.5 | |
| RibInterWR | Rib Intermuscular fat Weight Ratio (Rib intermuscular fat weight divided by the rib weight) | % | 8.8 ± 3.9 | |
| RibInterWM | Rib intermuscular fat weight divided by the muscle weight | % | 11.7 ± 5.1 | |
| RibW | Rib weight | g | 2417.1 ± 579.2 | |
| LTW | Weight of M. longissimus thoracis | g | 579.2 ± 74.6 | |
| | **Image analysis parameters** | | **CAF5R** | **CAF6R** |
| RibPortionArea | Rib Portion Area (Cut at 70 Degree) - Fig. 1-G | $cm^2$ | 177.2 ± 28.7 | 179.6 ± 31.5 |
| RibEyeArea | Rib Eye Area (hand drawn) - Fig. 1-G | $cm^2$ | 31.3 ± 7.1 | 38 ± 9.1 |
| RibEyeDissArea | Dissected Rib Eye Area (minus a thichness of 1.5 mm similar to the real dissection) | $cm^2$ | 30.5 ± 7.1 | 37.1 ± 9.1 |
| TrapezInterArea | Trapezius Intermuscular Fat Area (Under M. trapezius thoracis) - Fig. 1-H | $cm^2$ | 1.5 ± 1.3 | 2 ± 1.3 |
| TrapezInterThick | Trapezius Intermuscular Fat Thickness (Under M. trapezius thoracis) processed as the Area divided by the Feret diameter- Fig. 1-H | cm | 0.4 ± 0.2 | 0.4 ± 0.2 |
| TrapezSubThick | Trapezius Subcutaneous Fat Thickness (Over M. trapezius thoracis) processed as the Area divided by the Feret diameter- Fig. 1-H | cm | 0.5 ± 0.3 | 0.4 ± 0.3 |
| RibEyeFAR | Fat Area Ratio in the Rib Eye | % | 4.5 ± 2.9 | 4.9 ± 3.7 |

(*continued on next page*)

**Table 2** (*continued*)

| Features | Description | Unit | Statistics | |
|---|---|---|---|---|
| | (marbling) - Fig. 1-G | | | |
| RibEyeDissFAR | Fat Area Ratio in the Dissected Rib Eye (marbling) | % | 4.7 ± 3 | 5.1 ± 4 |
| RibEyeDissFARCor | Fat Area Ratio in the Dissected Rib Eye with density correction (d = 0.9 for marbling and d = 1.1 for lean) | % | 3.9 ± 2.5 | 4.2 ± 3.4 |
| RibEyeFARMt | Fat Area Ratio in the Rib Eye (manual threshold) | % | 5.4 ± 4 | 5.7 ± 4.3 |
| RibEyePlus25InterFAR | Intermuscular Fat Area Ratio in the Rib Eye area + 25% portion - Fig. 1-G | % | 18.5 ± 6.5 | 18.3 ± 6.3 |
| RibEyePortion25InterFAR | Intermuscular Fat Area Ratio in the 25% area around the Rib Eye - Fig. 1-G | % | 43.2 ± 14.4 | 45.6 ± 15.1 |
| RibEyePlus25InterFARCor | Intermuscular Fat Area Ratio in the Rib Eye area + 25% portion, with density correction - Fig. 1-G | % | 15.7 ± 5.7 | 15.5 ± 5.6 |
| RibPortionFAR | Fat Area Ratio in the Rib portion - without distinction of intra or intermuscular - Fig. 1-H | % | 23.1 ± 6.1 | 25.5 ± 6.5 |
| FleckArea | Average marbling flecks area in the rib eye | $mm^2$ | 1.6 ± 0.9 | 1.9 ± 1.1 |
| FleckPeri | Average marbling flecks perimeter in the rib eye | mm | 4.4 ± 1.3 | 4.8 ± 1.4 |
| FleckNum | Number of marbling flecks in the rib eye | | 90.8 ± 49.6 | 93.5 ± 53.9 |

decision trees at training time and outputs the mean prediction of the individual trees (regression analysis). The *party* R package was employed because it was shown to be more efficient for predictions using highly correlated data [23]. Finally, the combination of the ClustOfVar and MLR methods was also used to predict gold standard parameters. The ClustOfVar method was performed using the *ClustOfVar* R package [24]. This technique was developed specifically for identifying the synthetic variables that summarize the homogenous clusters. Each cluster is synthesized by one variable. The most relevant synthetic variables were then introduced in the MLR prediction model.

To evaluate the prediction models, we compared the mean and standard deviation (SD) of the predicted and measured values. We calculated the coefficient of determination ($R^2$), the root mean square error of prediction (RMSEP) and the ratio performance deviation (RPD) in both the calibration and validation sets. Models with the highest $R^2$ and RPD values and the lowest RMSEP were considered the most accurate. Karoui [25] used the $R^2$ values to define four robustness classes: poor ($R^2 < 0.66$), approximate ($0.66 <= R^2 <= 0.81$), good ($0.82 <= R^2 <= 0.90$), and excellent ($R^2 >= 0.91$). Models with an RPD > 2 provide predictions with good accuracy [26–28].

To discuss the parameters identified as important for the prediction models, the variable importance (VIP) criterion was used for both the SPLS and RF methods. Interest is mainly focused on these two methods that conserve the original variables and also provide the best predictive results. For SPLS, this VIP criterion must exceed 1. For the RF method, there is no predefined threshold. We calculated the cumulative ordered variable importance (decreasing order) to provide an increasing curve, and we selected the features that contributed to a significant increase in VIP values. The variables that occurred beyond the chosen threshold did not provide meaningful information in terms of prediction. For the ClustOfVar + MLR method, we chose the significant synthetic variables identified by the MLR model.

## 3. Results

### 3.1. IMF and rib weight results

Statistics of the slaughtered animals and their carcass traits are presented in Table 1. Bovines were chosen to represent the beef market in France and Europe in terms of marbling and rib composition with a wide range of data distributions from very lean to very fat ribs or LT. Consequently, even though the average age at slaughter ranged from 16.9 to 73 months, the hot carcass weight (average of 350 kg) and degree of adiposity of carcasses (average of 2.9) assayed by the EUROP grading system were within a similar range of values among the four classes of bovines. The conformation scores were, however, different between the four classes of bovines with the following class order: beef young bulls > beef other > dairy young bulls = dairy others. Statistics of the gold standard features assayed by chemical analysis or by rib dissection and weighting are presented in Table 2 and Fig. 2. The average IMF content was 6.6% in LT (Table 2), with a distribution of the animals around this average (Fig. 2), with both very lean (less than 2%) and very fat LT muscle (>16%). The total rib fat and muscle ratios averaged 12.3 and 66.1%, respectively with a range of approximatively 39% and 7%. Of the 12.3% total rib fat ratio, 8.8% was composed of intermuscular fat. The average weights of the rib and LT were 2.42 kg and 287.7 g, respectively. These data followed a normal distribution around the means (Fig. 2).

### 3.2. Performances of the developed open-access computer image analysis (CIA) method

The rib images from 130 half carcasses (29 right side, 101 left side) were captured by six operators (only one operator per each day of image acquisition) in two slaughterhouses from January 2018 to January 2019. None of the 130 CAF5R images and 129 CAF6R images (one forgotten) were unanalyzable (blurry, saturated or poorly framed). A first expert operator processed all the images, using the ImageJ program, in 4.3 and 4.7 min on average per image for the CAF5R and CAF6R images, respectively. A second expert operator visually validated all the saved images resulting from the overlay of a segmented image on the original image. Among the 259 analyzed images, one needed to be entirely reanalyzed, nine needed to be prefiltered because the polarizer was forgotten, and forty-two CAF6R images had poor subcutaneous fat detection because the algorithm failed to distinguish white fat from the white table. The image resolution ranged from 85 μm/pixel (±23%) to 97 μm/pixel (±20%) for the CAF5R and CAF6R images, respectively. Statistics of the image analysis parameters are presented in Table 2. All values are comparable between CAF5R and CAF6R except for the ribeye area, which is greater on CAF6R (38 $cm^2$ on average) than on CAF5R (32 $cm^2$ on average). This result is consistent with the fact that the LT muscle cross section is smaller in the cranial than in the caudal direction.

### 3.3. Correlations between gold standards and image analysis features for IMF and rib composition

Correlation matrices between all 26 quantitative data listed in the same order as Table 2 and including the three groups of measurements (the animal and carcass traits, the gold standard parameters and the image analysis parameters) were produced from data assayed on the CAF5R and CAF6R rib faces (Fig. 3). First, both matrices are visually

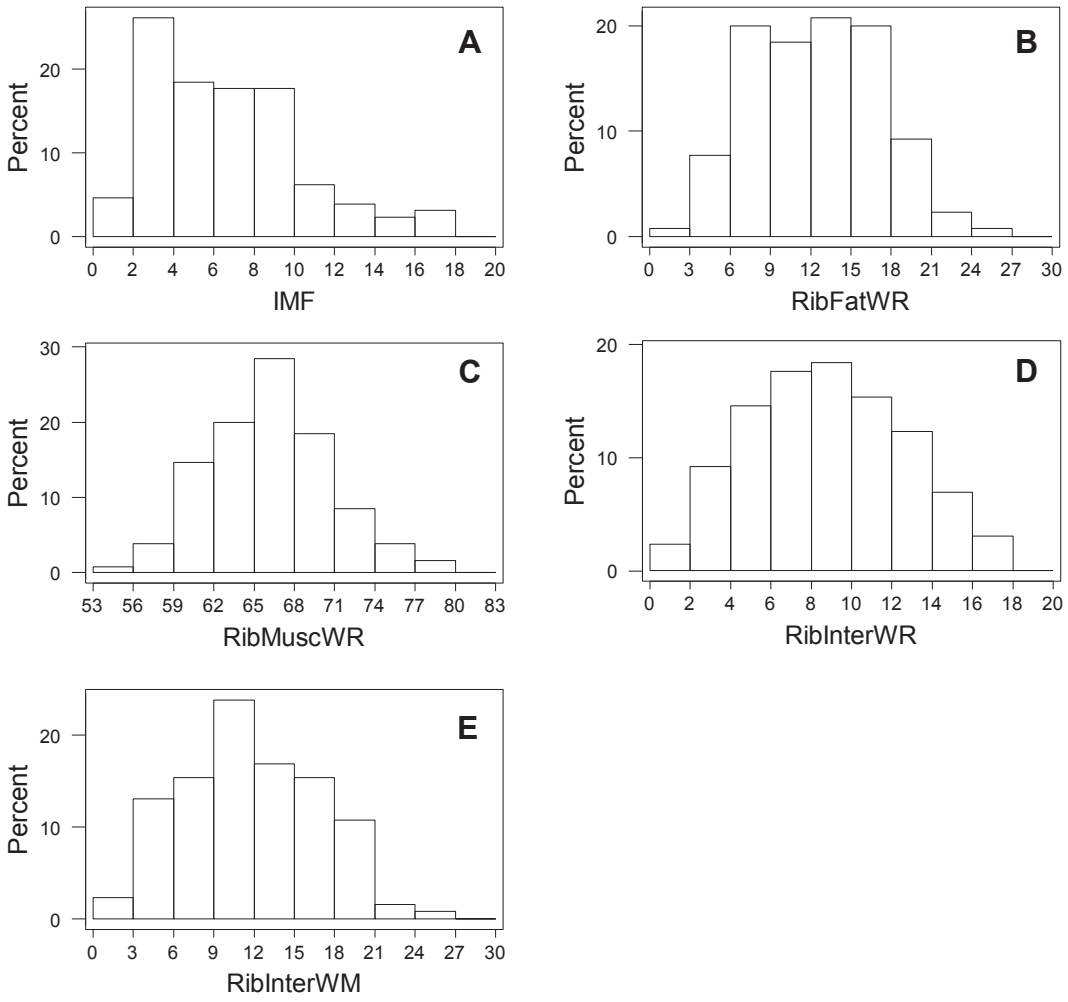


**Fig. 2.** Distributions (%) of (A) intramuscular fat in the *longissimus thoracis* muscle (IMF), (B) rib fat weight ratio (RibFatWR), (C) rib muscle weight ratio (RibMuscWR), (D) rib intermuscular fat weight ratio (RibInterWR) and (E) rib intermuscular fat weight divided by the muscle weight (RibInterWM).

similar, indicating similar relationships between (1) the rib faces and (2) the measurements and group of measurements regardless of the rib face, even if both faces may be visually different (Fig. 1-C and D).

The correlation coefficients were high between the gold standard and the image analysis data. Indeed, the correlations between IMF content and marbling percentage assayed by CIA methods are reported in Fig. 3. The values ranged from r = 0.76 when marbling was assayed automatically (RibEyeFAR, RibEyeDissFAR, RibEyeDissFARCor) to r = 0.79 when a manual threshold (RibEyeFARMt) was added for the analyses of the CAF5AR pictures. The correlations were better when the IMF content was compared to the intramuscular fat areas assayed on the pictures from the CAF6AR side and ranged from 0.85 to 0.87. The best correlations between the lean rib ratio estimated by dissection and image features were negative correlations (r = -0.61 to −0.64) between RibMuscWR and the intermuscular fat areas (RibEyePlus25InterFAR, RibEyePortion25InterFAR, RibEyePlus25InterFARCor). The correlation coefficients obtained between the fat tissue areas (RibEyePlus25InterFAR, RibEyePortion25InterFAR, RibEyePlus25InterFARCor, RibPortionFAR) and weights (RibFatWR) ranged from 0.50 to 0.54 and from 0.65 to 0.67 when assayed on the CAF5AR and CAF6AR pictures. Unexpectedly, the correlations were close when the areas assayed in the 25% enlarged area surrounding the muscle rather than the entire rib were considered. Last, high correlation values appeared between the different ways the fat area ratios were expressed: r = 0.87 to 1 for the intramuscular fat area ratio (RibEyeFAR, RibEyeDissFAR, RibEyeDissFARCor, RibEyeFARMt) and r = 0.76 to 1 for the intermuscular fat area ratio (RibEyePlus25InterFAR, RibEyePortion25InterFAR, RibEyePlus25InterFARCor, RibPortionFAR). The two categories of fat area ratios (intramuscular and intermuscular) were positively correlated (r = 0.49 to 0.65). In contrast, the negative correlations logically concerned the lean proportion. We have noted that the coefficients of correlation were generally lower/similar for young bulls or higher for “others” bovines than for the total population (130 bovines) of the study. We chose to present the correlation coefficients for the total population in order to keep the highest robustness provided by the high variation range considered.

### 3.4. Prediction of IMF and rib composition thanks to image and animal features

Tables 3 and 4 show the prediction results for the IMF and rib composition from the cranial (CAF6R) and caudal (CAF5R) faces of the 6th rib cut estimated by image analysis. The data obtained from the image analysis features of the CAF6R provide a prediction accuracy higher than that provided by the image analysis features of the CAF5R, for both IMF percent and rib fat composition. Moreover, the prediction accuracies and errors of prediction were very similar regardless of the methods of prediction used to predict one gold standard feature, i.e., IMF content, RibFatWR, RibMuscWR, RibInterWR, and RibInterWM. By combining the animal and image analysis features of the CAF5R, the best predictions with the lowest prediction errors were obtained by SPLS with a good precision of the prediction, since the $R^2$ was 0.77, RPD > 2,

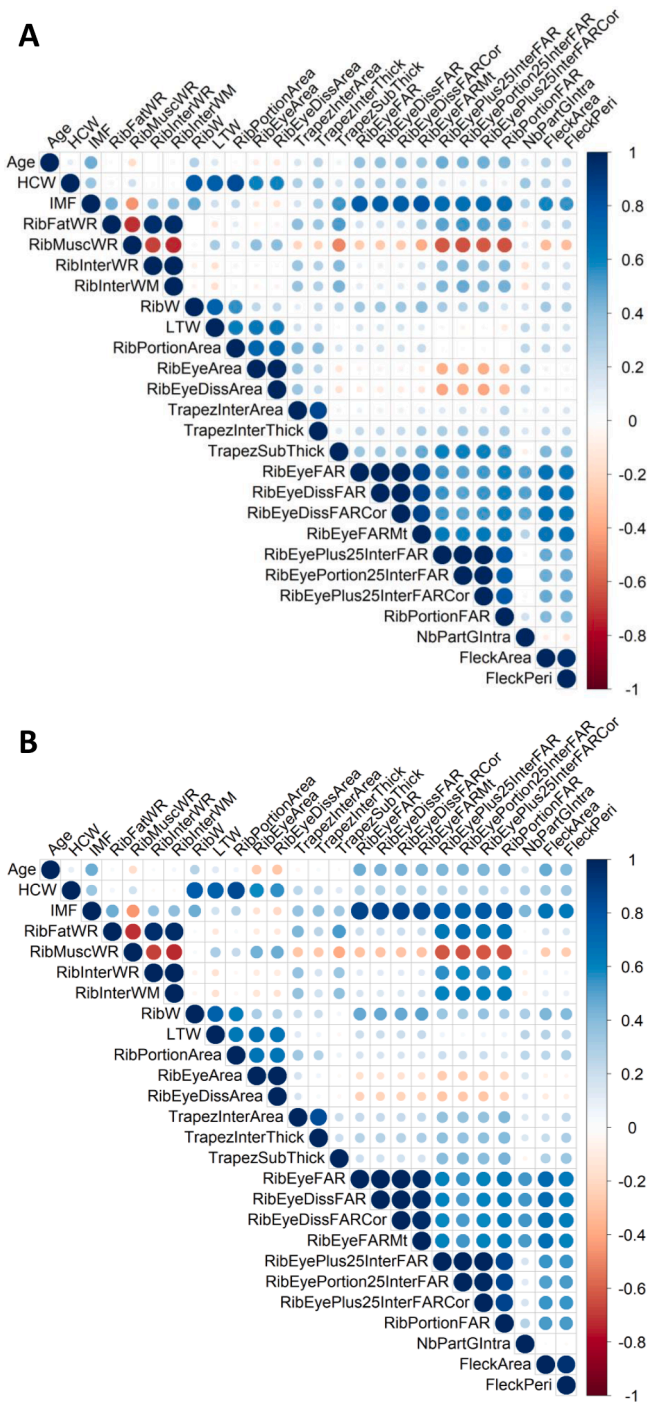


**Fig. 3.** Correlation matrix of all measurements. Animal and carcass traits, gold standard parameters and image analysis parameters for (A) CAF5R and (B) CAF6R. The scale on the right indicates the correlation level from red (r = -1) to blue (r=+1), which is graphically enhanced by the size of each colored disk. For instance, the IMF is highly and positively correlated with most of the image analysis parameters that rely on fat area measurements. In contrast, the RibMusWR is negatively correlated with most of the measurements except for both anatomic areas of interest (the rib eye and the rib portion). (For interpretation of the references to color in this figure legend, the reader is referred to the web version of this article.)

and the RMSEP value was 1.44% for IMF. Random forest modeling for the rib composition features provided approximate predictions with $R^2$ values ranging from 0.72 to 0.75, RPD ranging from 1.87 to 1.98 and RMSEP ranging from 2 to 2.7% for RibFatWR, RibMuscWR, RibInterWR, and RibInterWM (Table 3). By combining the animal and image analysis features of the CAF6R, the best predictions with the lowest prediction errors were obtained by SPLS for both IMF percent and rib composition. The predictions were very good with an $R^2$ value of 0.90, an RPD value of 3.14, and an RMSEP value equal to 0.92% for IMF. Regarding rib composition, the $R^2$ values ranged from 0.72 to 0.86, the RPD values ranged from 2.12 to 2.68, and the RMSEP values ranged from 1.9 to 2.1% for RibFatWR, RibMuscWR, RibInterWR, and RibInterWM (Table 4).

Fig. 4 shows a list of variables ranked according to their importance in the prediction models, with both SPLS and RF methods. Of the 6 and 17 features related to animal or image analyses, 3, namely, TrapezInterArea, TrapezInterThick and FleckNum, did not provide any improvement regardless of the method used for the prediction of IMF or rib composition. Among the most used features for the prediction of IMF (Fig. 4), 5 features (RibEyeDissFARCor, RibEyeFARMt, RibEyePlus25InterFARCor, RibEyeDissFAR, RibEyeFAR) related to the fat area ratio within the LT of the pictures contributed the most to the best models for both methods (SPLS or Random Forest) and the two sides of the rib (CAF5R and CAF6R); however, the variables presented a different order. Regardless of the models and the sides of the rib analyzed, RibEyePortion25InterFAR, TrapezSubThick, RibPortionFAR, and BeefYoungBulls were the animal and image analysis features used to predict the total rib fat ratio, and they logically combined areas for total, intermuscular and subcutaneous fat tissues. Four animal and image analysis features used in the four model results were considered the most representative features for evaluating the rib muscle ratio (RibMuscWR), namely, RibEyePlus25InterFAR, RibEyePortion25InterFAR, HCW, and RibPortionFAR related to carcass weight and mainly intermuscular fat areas (Fig. 4). Two animal features (BeefYoungBulls, HCW) plus two image analysis features (RibEyePortion25InterFAR, RibPortionFAR) appeared in the best models to predict either the rib intermuscular fat ratio related to the rib weight (RibInterWR) or the muscle weight (RibInterWM).

## 4. Discussion

An original computerized image analysis method was developed under open source software used the image analysis settings previously described for the classification of marbling [9,29] and rib composition [12,13] with new settings and conditions for image acquisition. Of the new settings for image analysis, we added simultaneous automatic detection of intra- and intermuscular areas using the Li segmentation method [20] but applied it to a specific area around the LT muscle enlarged by 25%. This method was proven efficient for marbling and rib composition analyses, considering the very good correlation and prediction results. Of note, relatively few studies published to date have reported CIA data and the correlation between the areas of fat or muscle tissue and the values assayed by gold standard methods (Soxlhet method or rib dissection), and most of these previous studies were carried out under calibrated and controlled conditions for image acquisition. Thus, the choice to develop a CIA method with very few fixed conditions in picture acquisition adds additional difficulties for image computerization, which were overcome to produce accurate quantification of areas as good predictors of marbling or rib composition. The choices of new settings for image acquisition to overcome such difficulties were the use of (1) a small and light squared scale usable even directly on a carcass and (2) two polarizing filters adaptable to a smartphone and a digital camera. Based on the lack of noninterpretable images, these solutions were proven to overcome the main problems of rib photography, which are the light reflection from wet tissue and the geometrical calibration of the image to be analyzed. With a recent smartphone (>10 Mpixels) equipped with such a polarized strobe, almost all pictures were analyzable even in a slaughterhouse with low lighting and hanging carcasses that moved. Nevertheless, this solution also has the following three limitations: (1) the ambient direct lighting level needs to be

**Table 3**
Measured means and standard deviations (Sd), predicted means and standard deviations, mean bias, residual standard deviation (Sd res), coefficient of determination ($R^2$), ratio of performance to deviation (RPD), residual root mean square error of prediction (RMSEP) for IMF, RibFatWR, RibMuscWR, RibInterWR, RibInterWM, using sparse partial least squares (SPLS) analysis, random forest (RF) analysis, and multiple linear regression on clusters of variables (Clust. MLR) on the validation dataset of 84 CAF5R images.

| | n | Measured mean | Measured Sd | Predicted mean | Predicted Sd | Bias | Sd res. | $R^2$ | RPD | RMSEP |
|---|---|---|---|---|---|---|---|---|---|---|
| IMF (%) | | | | | | | | | | |
| SPLS | 84 | 5.66 | 2.97 | 5.50 | 2.56 | −0.17 | 1.44 | 0.77 | 2.06 | 1.44 |
| RF | 84 | 5.66 | 2.97 | 5.51 | 2.21 | −0.15 | 1.56 | 0.73 | 1.91 | 1.59 |
| Clust. MLR | 84 | 5.66 | 2.97 | 5.57 | 2.50 | −0.09 | 1.45 | 0.77 | 2.05 | 1.45 |
| RibFatWR (%) | | | | | | | | | | |
| SPLS | 84 | 11.777 | 4.50 | 11.51 | 3.67 | −0.26 | 2.52 | 0.69 | 1.78 | 2.52 |
| RF | 84 | 11.77 | 4.50 | 11.67 | 3.08 | −0.10 | 2.28 | 0.75 | 1.98 | 2.40 |
| Clust. MLR | 84 | 11.77 | 4.50 | 11.51 | 3.70 | −0.26 | 2.58 | 0.67 | 1.74 | 2.58 |
| RibMuscWR (%) | | | | | | | | | | |
| SPLS | 84 | 67.52 | 3.81 | 67.48 | 3.00 | −0.04 | 2.22 | 0.67 | 1.72 | 2.21 |
| RF | 84 | 67.52 | 3.81 | 67.47 | 2.62 | −0.05 | 1.96 | 0.74 | 1.95 | 2.05 |
| Clust. MLR | 84 | 67.52 | 3.81 | 67.54 | 2.66 | 0.02 | 2.43 | 0.60 | 1.57 | 2.43 |
| RibInterWR (%) | | | | | | | | | | |
| SPLS | 84 | 8.43 | 3.85 | 8.07 | 3.04 | −0.36 | 2.21 | 0.67 | 1.74 | 2.23 |
| RF | 84 | 8.43 | 3.85 | 8.19 | 2.55 | −0.24 | 2.06 | 0.72 | 1.87 | 2.18 |
| Clust. MLR | 84 | 8.43 | 3.85 | 8.16 | 3.02 | −0.26 | 2.21 | 0.68 | 1.74 | 2.22 |
| RibInterWM (%) | | | | | | | | | | |
| SPLS | 84 | 11.03 | 4.89 | 10.72 | 3.92 | −0.31 | 2.70 | 0.70 | 1.81 | 2.70 |
| RF | 84 | 11.03 | 4.89 | 10.80 | 3.29 | −0.23 | 2.56 | 0.73 | 1.91 | 2.71 |
| Clust. MLR | 84 | 11.03 | 4.89 | 10.75 | 3.90 | −0.28 | 2.76 | 0.69 | 1.77 | 2.76 |

**Table 4**
Measured means and standard deviations (Sd), predicted means and standard deviations, mean bias, residual standard deviation (Sd res), coefficient of determination ($R^2$), ratio of performance to deviation (RPD), residual root mean square error of prediction (RMSEP) for IMF, RibFatWR, RibMuscWR, RibInterWR, RibInterWM, using sparse partial least squares (SPLS) analysis, random forest (RF) analysis, and multiple linear regression on clusters of variables (Clust. MLR) on the validation dataset of 84 CAF6R images.

| | n | Measured mean | Measured Sd | Predicted mean | Predicted Sd | Bias | Sd res. | $R^2$ | RPD | RMSEP |
|---|---|---|---|---|---|---|---|---|---|---|
| IMF (%) | | | | | | | | | | |
| SPLS | 84 | 5.69 | 2.91 | 5.64 | 2.82 | −0.06 | 0.93 | 0.90 | 3.14 | 0.92 |
| RF | 84 | 5.69 | 2.91 | 5.60 | 2.37 | −0.09 | 0.97 | 0.89 | 2.99 | 1.04 |
| Clust. MLR | 84 | 5.69 | 2.91 | 5.65 | 2.75 | −0.05 | 0.95 | 0.89 | 3.06 | 0.94 |
| RibFatWR (%) | | | | | | | | | | |
| SPLS | 84 | 11.92 | 4.54 | 11.62 | 3.95 | −0.29 | 1.80 | 0.84 | 2.52 | 1.83 |
| RF | 84 | 11.92 | 4.54 | 11.61 | 3.22 | −0.31 | 1.98 | 0.81 | 2.29 | 2.17 |
| Clust. MLR | 84 | 11.92 | 4.54 | 11.72 | 3.93 | −0.20 | 2.07 | 0.79 | 2.19 | 2.07 |
| RibMuscWR (%) | | | | | | | | | | |
| SPLS | 84 | 67.26 | 3.93 | 67.24 | 3.08 | −0.02 | 2.12 | 0.71 | 1.85 | 2.12 |
| RF | 84 | 67.26 | 3.93 | 67.30 | 2.71 | 0.04 | 2.23 | 0.68 | 1.76 | 2.28 |
| Clust. MLR | 84 | 67.26 | 3.93 | 67.26 | 3.04 | 0.00 | 2.20 | 0.69 | 1.78 | 2.20 |
| RibInterWR (%) | | | | | | | | | | |
| SPLS | 84 | 8.54 | 3.89 | 8.25 | 3.34 | −0.29 | 1.48 | 0.86 | 2.63 | 1.52 |
| RF | 84 | 8.54 | 3.89 | 8.27 | 2.78 | −0.28 | 1.58 | 0.84 | 2.46 | 1.78 |
| Clust. MLR | 84 | 8.54 | 3.89 | 8.28 | 3.25 | −0.26 | 1.76 | 0.80 | 2.21 | 1.78 |
| RibInterWM (%) | | | | | | | | | | |
| SPLS | 84 | 11.23 | 5.03 | 10.89 | 4.30 | −0.33 | 1.88 | 0.86 | 2.68 | 1.93 |
| RF | 84 | 11.23 | 5.03 | 10.88 | 3.51 | −0.34 | 2.07 | 0.83 | 2.42 | 2.35 |
| Clust. MLR | 84 | 11.23 | 5.03 | 10.97 | 4.22 | −0.26 | 2.18 | 0.81 | 2.30 | 2.21 |

moderate, (2) the rib must be cut cleanly and flat and (3) a red table is preferred to a white table to help with the automatic detection of subcutaneous fat. This study used a high-end smartphone that naturally became a mid-range model at the end of the image acquisition period. Thus, today, this phone would be easily replaceable by any smartphone. With a good imager that was enriched with only polarizing filters and a small laminated scale, we proved that it was possible to capture an image that could be quantitatively analyzed by an algorithm, even under real industrial conditions, while most past studies needed more controlled conditions. Only the ergonomics of the smartphone in a slaughterhouse was problematic and should be improved. Last, the use of a smartphone as a marbling sensor brings many advantages over dedicated instruments for fat quantification, such as NIRS, ultrasound or tomography. First, this method is a cost-effective solution since there is no need to develop a specific device. Measurement is reduced to software image analysis that can be embedded in the smartphone. Then, a smartphone-based measurement tool would be easy for most people to approach since most people have experience using a smartphone and have one.

In addition to the originality of the material used, including the developed image acquisition and CIA methods, the present publication is original due to the use of a large number of ribs with a wide range of marbling variability, which complements the results obtained by comparing extreme groups [29]. An additional originality is the 17 features produced in less than 5 min by a semiautomatic method that should minimize the analyst variability as well as errors related to human visual perception of marbling, which have already been pointed out as a major drawback for a true evaluation of marbling from images [10]. Regarding the application domain of the present CIA method, the accuracy of the method is high for lean meat, which thus complements the very few publications reporting IMF [29,30] or rib composition [13] CIA data in European breeds. Indeed, the present CIA method was

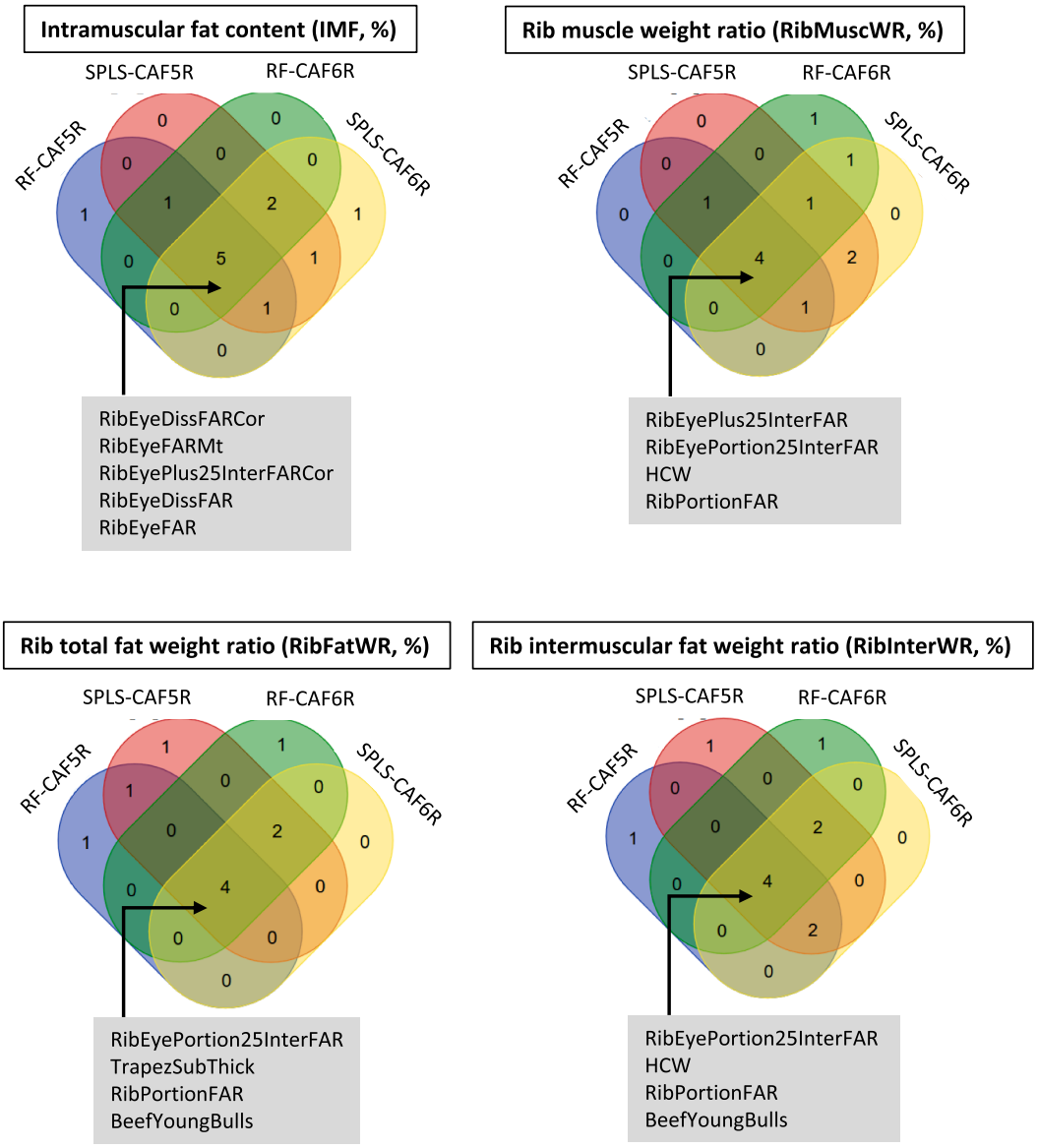


**Fig. 4.** Animal and image features used to predict IMF or lean and fat rib composition using sparse partial least squares (SPLS) analysis and random forest (RF) analysis on the validation dataset of 84 CAF5R images and 84 CAF6R images. Animal and image features retrieved for prediction.

developed from bovines with IMF contents in LT and total rib fat that ranged from 1.56 to 17.59% and from 2.08 to 24.45%, respectively. The dataset comprised young bulls, steers, heifers and cows, mostly from continental beef (Angus × Salers, Charolais, Rouge des Près, Salers as well as beef crossbreeds) and dairy (Prim'Hosltein, Normande, Montbéliarde as well as dairy crossbreeds) breeds. The high accuracy of the present CIA method is testified by the good to high correlations between the gold standard and the image analysis measures. Indeed, the present correlation coefficients obtained for marbling values (from 0.79 to 0.87) between the reference Soxhlet method and image analysis were higher than those obtained for Italian crossbred or Angus heifers ($r = 0.62$; [29]). Moreover, these correlations were similar or lower than those previously reported from fatter breeds typically found in US ($r = 0.82$ to 0.85, [6]) or Asian ($r = 0.93$ to 0.96 [7,8]) markets. The lower correlations repeatedly reported in slightly marbled European breeds than those in highly marbled American or Asian breeds may be explained by a more difficult and less accurate quantification of marbling by both image processing and chemical methods, as well as by a lower range of adiposity variation in European breeds, by a differences among the number of bovines included in the studies compared or by the rib number. Moreover, the present CIA methods evaluated the lean or fat proportion within a rib with good precision, as indicated by the good correlation coefficients between the percentages of separable lean and fat tissues assayed by CIA and rib dissection. The present correlation coefficients obtained between the image analysis information and rib dissection, both for fat and lean rib proportions, were higher (from 0.54 to 0.66) than those reported by Santos [13] in European lean bulls (from 0.41 to 0.59, $n = 180$, 9-10th and 12-13th rib interfaces) but similar or lower (from 0.68 to 0.82, $n = 44$, 12-13th rib interface) than those reported by Cross et al. [31] in early and late maturing American bulls and steers. Most of the correlations were positive, which confirms a dependency between the fat deposited in the different anatomic regions mainly related to the age at slaughtering [32,33]. Last, as already stated by Santos et al. [13], the assayed areas differed between the sides of the rib because the cross-sectional areas were not constant along the cranial-caudal axis of the ribs. Collectively, these very good correlations between areas and gold standard values, as well as the expected good inverse correlations (from −0.61 to −0.64) between muscle and fat areas, highlighted the accuracy of the image features produced by the present method to simultaneously evaluate IMF content and rib composition.

With the aim of designing a complete computer vision device, we thus used the aforementioned image features to produce predictive models for IMF content and rib composition. The combination of features from image analyses and animals was powerful to provide predictive models with high accuracy, which is in line with the results of the predictions already developed for carcass composition [12,34]. Using RMSEP and RPD as indicators of the prediction accuracy ($R^2$) of the models, the developed models predicted the IMF content and the proportion of total or intermuscular fat better than the muscle (or lean) proportion. This difference may be explained by the larger variations in IMF or rib fat proportion than those in muscle proportion within our datasets, as already reported by Pabiou et al. [34], depicting less accurate predictions of features with limited variations than those of features with large phenotypic variations. Moreover, the best predictions as measured by a high accuracy ($R^2$), low RMSEP and high RPD were obtained from CAF6R data. For IMF prediction, 4 out of the 5 features retrieved in the four models were related to the proportions of the segmented intramuscular fat area within the rib eye areas. This result is consistent with the generally admitted fact that IMF content is associated with the characteristics (surface, numbers…) of marbling flecks measured by image analysis [6,7,29]. More surprisingly, an additional feature related to the intermuscular fat area within the 25% surrounding area was shown to contribute to the prediction of IMF content. The reason for the contribution of this feature may be that marbling deposition is strongly related to intermuscular fat deposition [33]. The coefficients of determination obtained with data from the CAF6R face for predicting the percentage of fat (0.79 to 0.86 for total and intermuscular fat tissues) and lean (from 0.68 to 0.71) are similar or higher than those reported by Santos [13] in European lean bulls (lean, 0.53; fat 0.68–0.76). To the best of our knowledge, the unique CIA method that was developed to predict rib composition produced 6 image features [13], which made comparative analysis of the best reported predictors difficult. In the present study, regardless of the face of the rib and the predictive method, the best predictors of the rib lean proportion were 3 features related to the intermuscular fat areas and the HCW. In the study by Santos [13], the best predictors for the rib lean proportion were related to either muscle or bone areas depending on the face of the rib that was analyzed, and predictions were improved when the values for carcass weight were used. These results are consistent with the well-known close relations between muscle, fat and bone mass in bovines [32,33]. The four predictors for the total fat rib proportion revealed that regardless of the face of the rib and the predictive method that was used, there were areas that were logically related to intermuscular, subcutaneous and total fat in combination with the indication of the type of bovine, such as beef young bulls. Four predictors for the intermuscular fat rib proportion were also found regardless of the face of the rib and the predictive method that was used, and they were related to intermuscular and total areas, the HCW and again the indication of the type of bovine, such as beef young bulls. The reason for the contribution of the beef young bulls feature to the predictive models for total and intermuscular fats can probably be explained by the fact that beef young bulls are very lean and thus very different from the other bovine types. Overall, the very good performances of the prediction models obtained by combining several features and both animal and CIA data are in line with previously published results [13,34,35]. This finding is consistent with the fact that the deposition of fats relative to muscle is strongly dependent on the age, sex and breed of the animals [33]. The increase in performance by adding animal features that are easy to assay and at low costs is thus a strategy that could be chosen to predict meat or carcass characteristics.

## 5. Conclusions

The results of this study showed that both marbling and rib composition evaluations and predictions are feasible using inexpensive technologies, which would be easy to implement for industry purposes. The best prediction results were obtained by combining image analysis features related to the total, intermuscular, subcutaneous or intramuscular fat areas assayed over the entire rib surface or only the loin rib eye plus 25%, plus animal features, mainly HCW and the type of bovine (beef young bulls). For the beef industry, the convenience of working on either the carcass or the 6th rib sampled or analyzing the entire rib surface or only the loin rib eye plus 25% should be evaluated depending on the time cost relative to the prediction purposes. This method and the features provided are thus accurate enough to develop algorithms compatible with smartphone applications.

The ability to accurately predict IMF or rib fat composition has multiple applications. First, it provides an opportunity for slaughterhouses to quantify the value of the LT based on its marbling content, a major driver of consumer satisfaction. Second, the 6th rib composition is strongly related to the carcass composition; thus, the predicted rib composition could be used to quantify the value of the carcass, which may subsequently be used to pay the producer. Third, genetic variation exists in marbling deposition and rib composition; thus, the routine availability of data produced by the present CIA method should facilitate the routine estimation of bovine breeding values according to fat deposition. Finally, accurate prediction of marbling and rib composition aids in the evaluation of production systems or diets without the associated expenses of chemical analysis or dissection.

## Funding

This work was supported by the Special Assignment Account “Agricultural and Rural Development” (CASDAR) of the French Ministry of Agriculture, Agrifood and Forestry, project CASDAR RT 1620 Meat@ppli, available at http://www.idele.meat@pply.fr.

## CRediT authorship contribution statement

**Bruno Meunier:** Conceptualization, Data curation, Formal analysis, Methodology, Software, Visualization, Writing - original draft. **Jérôme Normand:** Funding acquisition, Project administration, Resources, Supervision, Writing - review & editing. **Benjamin Albouy-Kissi:** Funding acquisition, Methodology, Resources, Writing - review & editing. **Didier Micol:** Conceptualization. **Mohammed El Jabri:** Formal analysis, Methodology, Software, Visualization, Writing - review & editing. **Muriel Bonnet:** Conceptualization, Funding acquisition, Supervision, Visualization, Writing - original draft.

## Declaration of Competing Interest

The authors declare that they have no known competing financial interests or personal relationships that could have appeared to influence the work reported in this paper.

## Acknowledgments

We are grateful for the contributions of slaughterhouse members for giving us access to carcasses. We also gratefully acknowledge S. Prache for the production of 18 young beef bulls, Q. Delahaye, A. Delavaud, S. Bardou-Valette (INRAE), L. Allais, E. Batany, T. Coadaou, A. Debant, M. Joubert and C. Malayrat (French Livestock Institute), for carcass pictures, image analyses, rib dissections or IMF assays. We acknowledge B. Picard for helpful discussion.

## References

[1] A. Listrat, B. Lebret, I. Louveau, T. Astruc, M. Bonnet, L. Lefaucheur, B. Picard, J. Bugeon, How muscle structure and composition influence meat and flesh quality, Sci. World J. 2016 (2016) 3182746, https://doi.org/10.1155/2016/3182746.
[2] E.R. Johnson, Marbling fat in beef, Meat Sci. 20 (4) (1987) 267–279, https://doi.org/10.1016/0309-1740(87)90082-9.

[3] D.W. Pethick, G.S. Harper, V.H. Oddy, Growth, development and nutritional manipulation of marbling in cattle: a review, Aust. J. Exp. Agr. 44 (7) (2004) 705–715, https://doi.org/10.1071/Ea02165.
[4] C.A. Boykin, L.C. Eastwood, M.K. Harris, D.S. Hale, C.R. Kerth, D.B. Griffin, A. N. Arnold, J.D. Hasty, K.E. Belk, D.R. Woerner, R.J. Delmore, J.N. Martin, D. L. VanOverbeke, G.G. Mafi, M.M. Pfeiffer, T.E. Lawrence, T.J. McEvers, T. B. Schmidt, R.J. Maddock, D.D. Johnson, C.C. Carr, J.M. Scheffler, T.D. Pringle, A. M. Stelzleni, J. Gottlieb, J.W. Savell, National Beef Quality Audit - 2016: Survey of carcass characteristics through instrument grading assessments, J. Anim. Sci. 95 (7) (2017) 3003–3011, https://doi.org/10.2527/jas.2017.1544.
[5] L.J. Farmer, D.T. Farrell, Review: beef-eating quality: a European journey, Animal 12 (11) (2018) 2424–2433, https://doi.org/10.1017/S1751731118001672.
[6] D.E. Gerrard, X. Gao, J. Tan, Beef marbling and color score determination by image processing, J. Food Sci. 61 (1) (1996) 145–148, https://doi.org/10.1111/j.1365-2621.1996.tb14745.x.
[7] K. Kuchida, S. Kono, K. Konishi, L.D. Van Vleck, M. Suzuki, S. Miyoshi, Prediction of crude fat content of longissimus muscle of beef using the ratio of fat area calculated from computer image analysis: comparison of regression equations for prediction using different input devices at different stations, J. Anim. Sci. 78 (4) (2000) 799–803.
[8] Y. Nakahashi, S. Maruyama, S. Seki, S. Hidaka, K. Kuchida, Relationships between monounsaturated fatty acids of marbling flecks and image analysis traits in longissimus muscle for Japanese Black steers, J. Anim. Sci. 86 (12) (2008) 3551–3556, https://doi.org/10.2527/jas.2008-0947.
[9] K. Chen, C. Qin, Segmentation of beef marbling based on vision threshold, Comput. Electron. Agr. 62 (2) (2008) 223–230, https://doi.org/10.1016/j.compag.2008.01.002.
[10] P. Jackman, D.W. Sun, P. Allen, Automatic segmentation of beef longissimus dorsi muscle and marbling by an adaptable algorithm, Meat Sci. 83 (2) (2009) 187–194, https://doi.org/10.1016/j.meatsci.2009.03.010.
[11] A.B. Karnuah, K. Moriya, N. Nakanishi, T. Nade, T. Mitsuhashi, Y. Sasaki, Computer image analysis for prediction of carcass composition from cross-sections of Japanese Black steers, J. Anim. Sci. 79 (11) (2001) 2851–2856, https://doi.org/10.2527/2001.79112851x.
[12] T. Nade, J.I. Saburi, T. Abe, T. Nakagawa, T. Okumura, S. Misumi, K. Saito, T. Kawamura, K. Fujita, Estimation of the carcass composition from a cross-section of the rib-loin from crossbred Japanese Black x Limousin F2 cattle by computer image analysis, Anim. Sci. J. 78 (6) (2007) 567–574, https://doi.org/10.1111/j.1740-0929.2007.00477.x.
[13] R. Santos, F. Pena, M. Juarez, C. Aviles, A. Horcada, A. Molina, Use of image analysis of cross-sectional cuts to estimate the composition of the 10th-11th-12th rib-cut of European lean beef bulls, Meat Sci. 94 (3) (2013) 312–319, https://doi.org/10.1016/j.meatsci.2013.03.018.
[14] R.J. Gove, Complementary metal-oxide-semiconductor (CMOS) image sensors for mobile devices, Woodh. Pub. Ser. Elect. 60 (2014) 191–234, https://doi.org/10.1533/9780857097521.2.191.
[15] S. Hosseinpour, A.H. Ilkhchi, M. Aghbashlo, An intelligent machine vision-based smartphone app for beef quality evaluation, J. Food Eng. 248 (2019) 9–22, https://doi.org/10.1016/j.jfoodeng.2018.12.009.
[16] M. Cruz-Fernandez, M.J. Luque-Cobija, M.L. Cervera, A. Morales-Rubio, M. de la Guardia, Smartphone determination of fat in cured meat products, Microchem. J. 132 (2017) 8–14, https://doi.org/10.1016/j.microc.2016.12.020.
[17] C.A. Schneider, W.S. Rasband, K.W. Eliceiri, NIH Image to ImageJ: 25 years of image analysis, Nat. Methods 9 (7) (2012) 671–675, https://doi.org/10.1038/nmeth.2089.
[18] N. Otsu, Threshold selection method from Gray-level histograms, IEEE Trans. Syst. Man. Cyb. 9 (1) (1979) 62–66, https://doi.org/10.1109/Tsmc.1979.4310076.
[19] J.N. Kapur, P.K. Sahoo, A.K.C. Wong, A new method for Gray-level picture thresholding using the entropy of the histogram, Comput. Vision Graph 29 (3) (1985) 273–285, https://doi.org/10.1016/0734-189x(85)90125-2.
[20] C.H. Li, P.K.S. Tam, An iterative algorithm for minimum cross entropy thresholding, Pattern Recogn. Lett. 19 (8) (1998) 771–776, https://doi.org/10.1016/S0167-8655(98)00057-9.
[21] X.J. Yang, E. Albrecht, K. Ender, R.Q. Zhao, J. Wegner, Computer image analysis of intramuscular adipocytes and marbling in the longissimus muscle of cattle, J. Anim. Sci. 84 (12) (2006) 3251–3258, https://doi.org/10.2527/jas.2006-187.
[22] F. Rohart, B. Gautier, A. Singh, K.A. Le Cao, mixOmics: An R package for 'omics feature selection and multiple data integration, PLoS Comput. Biol. 13 (11) (2017), e1005752, https://doi.org/10.1371/journal.pcbi.1005752.
[23] C. Strobl, A.L. Boulesteix, A. Zeileis, T. Hothorn, Bias in random forest variable importance measures: illustrations, sources and a solution, BMC Bioinf. 8 (2007) 25, https://doi.org/10.1186/1471-2105-8-25.
[24] M. Chavent, V.K. Simonet, B. Liquet, J. Saracco, ClustOfVar: an R Package for the clustering of variables, J. Stat. Softw. 50 (13) (2012) 1–16.
[25] R. Karoui, A.M. Mouazen, E. Dufour, R. Schoonheydt, J. de Baerdemaeker, Utilisation of front-face fluorescence spectroscopy for the determination of some selected chemical parameters in soft cheeses, Lait 86 (2) (2006) 155–169, https://doi.org/10.1051/lait:2005047.
[26] M. De Marchi, V. Toffanin, M. Cassandro, M. Penasa, Prediction of coagulating and noncoagulating milk samples using mid-infrared spectroscopy, J. Dairy Sci. 96 (7) (2013) 4707–4715, https://doi.org/10.3168/jds.2012-6506.
[27] P. Gottardo, M. De Marchi, M. Cassandro, M. Penasa, Technical note: Improving the accuracy of mid-infrared prediction models by selecting the most informative wavelengths, J. Dairy Sci. 98 (6) (2015) 4168–4173, https://doi.org/10.3168/jds.2014-8752.
[28] M. El Jabri, M.P. Sanchez, P. Trossat, C. Laithier, V. Wolf, P. Grosperrin, E. Beuvier, O. Rolet-Repecaud, S. Gavoye, Y. Gauzere, O. Belysheva, E. Notz, D. Boichard, A. Delacroix-Buchet, Comparison of Bayesian and partial least squares regression methods for mid-infrared prediction of cheese-making properties in Montbeliarde cows, J. Dairy Sci. 102 (8) (2019) 6943–6958, https://doi.org/10.3168/jds.2019-16320.
[29] E. Giaretta, A.L. Mordenti, G. Canestrari, N. Brogna, A. Palmonari, A. Formigoni, Assessment of muscle Longissimus thoracis et lumborum marbling by image analysis and relationships between meat quality parameters, PLoS ONE 13 (8) (2018), e0202535, https://doi.org/10.1371/journal.pone.0202535.
[30] L. Schulz, A. Sundrum, Assessing marbling scores of beef at the 10th rib vs. 12th rib of longissimus thoracis in the slaughter line using camera grading technology in Germany, Meat Sci 152 (2019) 116–120, https://doi.org/10.1016/j.meatsci.2019.02.021.
[31] H.R. Cross, D.A. Gilliland, P.R. Durland, S. Seideman, Beef carcass evaluation by use of a video image-analysis system, J. Anim. Sci. 57 (4) (1983) 908–917.
[32] T. Gotoh, E. Albrecht, F. Teuscher, K. Kawabata, K. Sakashita, H. Iwamoto, J. Wegner, Differences in muscle and fat accretion in Japanese Black and European cattle, Meat Sci. 82 (3) (2009) 300–308, https://doi.org/10.1016/j.meatsci.2009.01.026.
[33] M. Bonnet, I. Cassar-Malek, Y. Chilliard, B. Picard, Ontogenesis of muscle and adipose tissues and their interactions in ruminants and other species, Animal 4 (7) (2010) 1093–1109, https://doi.org/10.1017/S1751731110000601.
[34] T. Pabiou, W.F. Fikse, A.R. Cromie, M.G. Keane, A. Nasholm, D.P. Berry, Use of digital images to predict carcass cut yields in cattle, Livest Sci 137 (1–3) (2011) 130–140, https://doi.org/10.1016/j.livsci.2010.10.012.
[35] I. Munoz, M. Rubio-Celorio, N. Garcia-Gil, M.D. Guardia, E. Fulladosa, Computer image analysis as a tool for classifying marbling: a case study in dry-cured ham, J. Food Eng. 166 (2015) 148–155, https://doi.org/10.1016/j.jfoodeng.2015.06.004.